Aalborg Universitet

Aalborg University
DENMARK

Polymer Acceptors with Flexible Spacers Afford Efficient and Mechanically Robust All-Polymer Solar Cells

Genene, Zewdneh; Lee, Jin Woo; Lee, Sun Woo; Chen, Qiaonan; Tan, Zhengping; Abdulahi, Birhan A.; Yu, Donghong; Kim, Taek Soo; Kim, Bumjoon J.; Wang, Ergang

Polymer Acceptors with Flexible Spacers Afford Efficient and Mechanically Robust All-Polymer Solar Cells

Zewdneh Genene, Jin-Woo Lee, Sun-Woo Lee, Qiaonan Chen, Zhengping Tan, Birhan A. Abdulahi, Donghong Yu, Taek-Soo Kim,* Bumjoon J. Kim,* and Ergang Wang*

High efficiency and mechanical robustness are both crucial for the practical applications of all-polymer solar cells (all-PSCs) in stretchable and wearable electronics. In this regard, a series of new polymer acceptors (P_As) is reported by incorporating a flexible conjugation-break spacer (FCBS) to achieve highly efficient and mechanically robust all-PSCs. Incorporation of FCBS affords the effective modulation of the crystallinity and pre-aggregation of the P_As, and achieves the optimal blend morphology with polymer donor (P_D), increasing both the photovoltaic and mechanical properties of all-PSCs. In particular, an all-PSC based on PYTS-0.3 P_A incorporated with 30% FCBS and PBDB-T P_D demonstrates a high power conversion efficiency (PCE) of 14.68% and excellent mechanical stretchability with a crack onset strain (COS) of 21.64% and toughness of 3.86 MJ m^{-3}, which is significantly superior to those of devices with the P_A without the FCBS (PYTS-0.0, PCE = 13.01%, and toughness = 2.70 MJ m^{-3}). To date, this COS is the highest value reported for PSCs with PCEs of over 8% without any insulating additives. These results reveal that the introduction of FCBS into the conjugated backbone is a highly feasible strategy to simultaneously improve the PCE and stretchability of PSCs.

1. Introduction

All-polymer solar cells (all-PSCs), consisting of a binary blend of a polymer donor (P_D) and a polymer acceptor (P_A), possess important advantages including enhanced morphological stability, improved mechanical flexibility, and better compatibility with large-area roll-to-roll production over PSCs based

on small molecule acceptors (SMAs).[1–8] The power conversion efficiency (PCE) of the all-PSCs has risen up to 16% very recently, driven by the rapid development of both new efficient P_Ds and polymerized small-molecule acceptors (PSMAs).[9–14] However, only a few all-PSCs with PCEs of over 13% have been reported, which is still much lower than those of the state-of-art SMA-based ones. More importantly, their mechanical properties are still far from the requirements on wearable devices (i.e., crack onset strain (COS) of at least 20–30% required).

The major hurdles that hamper the performance of all-PSCs based on PSMAs are the strongly phase-separated blend morphologies, driven by de-mixing of high molecular weight P_Ds and PSMAs, resulting in un-optimized charge generation and transport.[15,16] These un-optimal morphologies typically include numerous defect sites (i.e., sharp domain–domain interfaces and large polymer aggregates) in the blend film, limiting the mechanical robustness and stretchability with low COS.[17–19] In addition, the phase separation of polymer blends is affected by the aggregation and crystalline behaviors of the P_Ds and P_As. In particular, the PSMAs containing highly crystalline, rigid SMA unit typically possess very strong crystalline and aggregation properties, causing strongly phase-separated

Z. Genene, Q. Chen, B. A. Abdulahi, E. Wang
Department of Chemistry and Chemical Engineering
Chalmers University of Technology
Göteborg SE-412 96, Sweden
E-mail: ergang@chalmers.se

J.-W. Lee, Z. Tan, B. J. Kim
Department of Chemical and Biomolecular Engineering
Korea Advanced Institute of Science and Technology (KAIST)
Daejeon 34141, Republic of Korea
E-mail: bumjoonkim@kaist.ac.kr

The ORCID identification number(s) for the author(s) of this article can be found under https://doi.org/10.1002/adma.202107361.

S.-W. Lee, T.-S. Kim
Department of Mechanical Engineering
Korea Advanced Institute of Science and Technology (KAIST)
Daejeon 34141, Republic of Korea
E-mail: tskim1@kaist.ac.kr

D. Yu
Department of Chemistry and Bioscience
Aalborg University
Aalborg DK-9220, Denmark

D. Yu
Sino-Danish Center for Education and Research
Aarhus DK-8000, Denmark

E. Wang
School of Materials Science and Engineering
Zhengzhou University
Zhengzhou 450001, China

structure with excessive domain purity, thereby lowering both short-circuit current density (J_{sc}) and fill factor (FF) of all-PSCs.[17,20] Consequently, a variety of strategies including modification of the P_A structure and optimization of processing conditions have attempted to improve the blend morphology.[21–26]

Among these, ternary copolymerization provides effective means to modulate the solubility, optical property, energy level and aggregation behaviors of the P_As, and, thus, the blend morphology with the P_Ds.[27–32] For instance, Li et al. developed random ternary PSMAs to improve the solubility, molecular crystallinity, and morphology of the blends.[33] Their all-PSCs based on a P_A containing 30% ester-substituted thiophene as a third component exhibited better PCE and photostability as compared with those based on their parent P_A. However, a ternary copolymerization strategy has been rarely used to tune the aggregation behavior and molecular rigidity of PSMAs and the blend miscibility with P_D. This is particularly important to increase the mechanical robustness of the active layer by optimizing the domain sizes/purities and removing the morphological defects.[2,34,35]

The polymer:polymer blend films are supposed to have better mechanical properties than the polymer:SMAs-based ones. However, there are only very few studies about mechanical properties of all-PSCs based on PSMAs, and most of these devices reported exhibit low mechanical robustness (i.e., COS of less than 15%).[17,18] The low mechanical property is mainly due to their rigid and large fused-rings in such PSMA backbone, which causes excessive aggregation behaviors and unoptimal blend morphologies.[2,36] On the other hand, the planar and rigid fused-rings of the PSMAs are essential for achieving high light absorption, charge transport, and thereby high J_{sc} and PCE. Therefore, there is an urgent need to develop an effective method that achieves a balance between these two important influences in the PSMAs to combine mechanical robustness with high photovoltaic (PV) performance.

Recently, we reported two non-conjugated P_As, PF1-TS4 and PFY-2TS namely, with SMA (IDIC16 for the former and YBO-Br for the latter) linked by thioalkyl chains, which have comparable absorption coefficient and lowest unoccupied molecular orbital (LUMO) level as compared with IDIC16 and Y5.[37,38] The introduction of the "soft" flexible conjugation-break spacers (FCBS) of thioalkyl chains brings promising PV performance and morphological stability for either PF1-TS4 or PFY-2TS-based PSCs. Nevertheless, their mechanical properties are not explored. On the other hand, P_Ds containing FCBS have been developed very recently for SMA-based-PSCs.[39,40] However, the effect of the structure of P_As with FCBS on the PV performance and mechanical stretchability of the all-PSCs remains elusive.

Here, we developed a new and facile synthetic strategy for regulating the molecular rigidity and aggregation behavior of P_A through the introduction of FCBS, and achieved all-PSCs with high mechanical properties and PV performance at the same time. A series of Y5-based terpolymer acceptors consisting of 1,8-bis((5-(trimethylstannyl)thiophen-2-yl)thio)octane (TS8) as FCBS and thiophene were synthesized by random copolymerization. The incorporation of FCBS (i.e., non-conjugated thioalkyl chain) is found to significantly improve the solubility and molecular flexibility of P_As. Interestingly, this leads to the well-controlled temperature-dependent aggregation behavior,

resulting in enhanced crystallinity and electron mobility of P_A in thin films. As a result, all-PSCs based on PYTS-0.3 P_A incorporated with 30% of FCBS achieved a high PCE of 14.68%, which significantly outperform that of the all-PSC with PYTS-0.0 without FCBS (PCE = 13.01%) due to the enhanced exciton dissociation and suppressed monomolecular/trap-assisted recombination. Importantly, the mechanical robustness of PBDB-T:PYTS-0.3 blend is also significantly enhanced (COS = 21.64% and toughness = 3.86 MJ m⁻³) compared to those of the PBDB-T:PYTS-0.0 blend (COS = 18.84% and toughness = 2.70 MJ m⁻³), which represents one of the highest values among all-PSCs based on PSMAs so far. This study proposes a promising molecular design of PSMA as the P_A, affording the all-PSCs with high efficiency and mechanical properties suitable for stretchable and wearable devices.

2. Results and Discussion

2.1. Basic Material Properties

The chemical structures of the P_D and P_As are illustrated in **Figure 1**a. We selected PYTS-0.0 as the reference P_A because of its high optical absorption and fast charge-transport capabilities.[41] Poly[(2,6-(4,8-bis(5-(2-ethylhexyl)thiophen-2-yl)-benzo[1,2-*b*:4,5-*b*′]dithiophene))-*alt*-(5,5-(1,3′-di-2-thienyl-5,7′-bis(2-ethylhexyl)benzo[1,2′-*c*:4′,5′-*c*′]dithiophene-4,8-dione))] (PBDB-T) is employed as P_D in this study to construct complementary light absorption with a series of P_A.[42] FCBS was introduced into the backbone of PYTS-0.0 as a third component to systematically control the aggregation and crystalline properties of the P_As by alleviating their backbone rigidities (in pink in Figure 1b). A long 1,8-bis((5-(trimethylstannyl)thiophen-2-yl) thio)octane (TS8) segment was selected to provide sufficient backbone flexibility for the resulting P_As. The P_As were synthesized via Stille coupling polymerization by varying the molar ratios of thiophene (T) and TS8 donor units while fixing the content of Y5-OD-2Br (Scheme S1, Supporting Information). The resulting terpolymer acceptors were named PYTS-*x*, where *x* = 0.0, 0.1, 0.3, 0.5, and 1.0, respectively, denoting the mole fractions of the TS8 unit relative to the total donating moieties (T + TS8). The number-average molecular weights (M_ns) of PYTS-*x* are controlled to be similar among each other between 9–17 kg mol⁻¹ as determined by gel permeation chromatography (GPC) (**Table 1**).[43] The decomposition temperature (T_d, 5% mass loss) of the terpolymer acceptors was found as high as 340–344 °C in thermogravimetric analysis (TGA) (Figure S1a, Supporting Information), which indicates that the FCBS has little influence on the thermal properties of these terpolymers. The solubilities of the polymers were measured, which are summarized in Figure S2 and Table S1, Supporting Information. As anticipated, the solubility of the P_As clearly increased with increasing FCBS content in the polymer backbones. For example, the solubility of the P_As in hot chlorobenzene (CB) solution (at 80 °C) increased in the order of 7.2, 17.6, and 26.6 mg mL⁻¹ for the PYTS-0.0, PYTS-0.3, and PYTS-1.0, respectively (Table S1, Supporting Information).

The optical and electrochemical properties of the polymers are summarized in Figure 1d,e, Figure S1 (Supporting
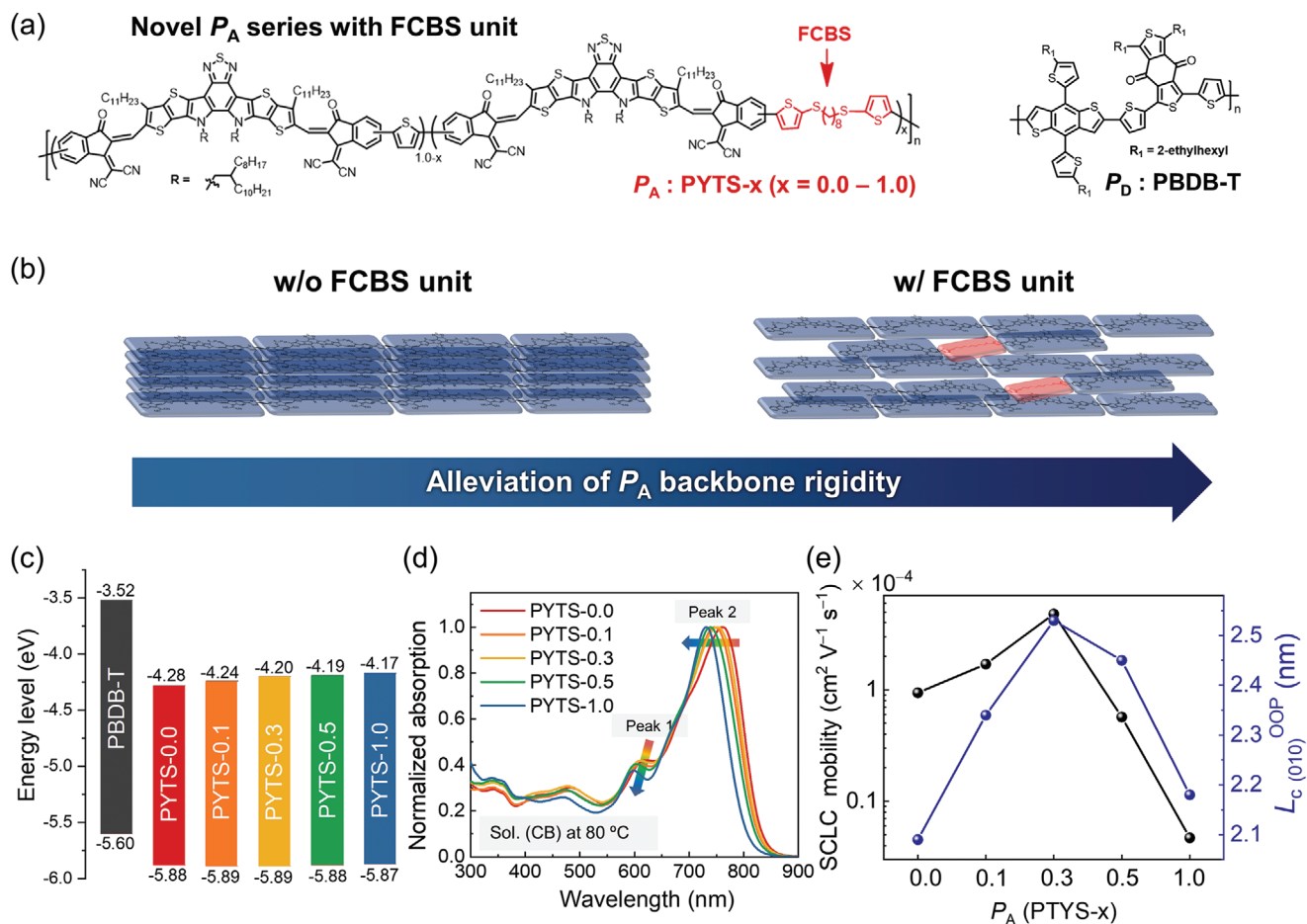
Figure 1. a) Chemical structures of P_As and P_D, b) Schematic illustrations for packing structures of the P_As without and with the FCBS unit, c) Molecular energy levels of P_D and P_As, d) Normalized absorption spectra of the P_As in CB solution at 80 °C, and e) $L_{c(010)}^{OOP}$ and SCLC electron mobility values of the P_As depending on their FCBS contents.

Information), and Table 1, respectively. Figure 1c shows the alignment of energy levels for the active materials, indicating that all of the P_As showed well-aligned highest occupied molecular orbital (HOMO) and LUMO levels with that of P_D for all-PSC operation. The P_As showed blueshifts for both shoulder-peak absorption in the 600–650 regime (peak 1) and maximum absorption wavelength (λ_{max}) in the 700–800 nm regime (peak 2) in the normalized UV–vis absorption at 80 °C in CB solution as the content of FCBS in the P_A increased (Figure 1d). This might arise from their molecular conformation changes via

rotation of sp^3 hybridized C–C single bonds within FCBS.[44,45] In PYTS-0.0, the fully conjugated and rigid backbone gives neither the Y5 nor the thiophene block enough freedom to twist, while the introduction of FCBS provides increased chain flexibility on P_A segments to twist. This results in above-mentioned blueshifted absorption spectra of P_As with FCBS in solution compared to those of PYTS-0.0. The absorption coefficient of the P_As in solution decreased with increasing FCBS content (Table S1, Supporting Information). On the other hand, all P_As showed similar λ_{max} and optical bandgap in film states,

Table 1. Basic structural, optical, and electrochemical properties of the active materials used in this study.

Polymer	M_n [kg mol^{-1}]	Đ	λ_{max}^{film} [nm][a]	E_g^{opt} [eV][b]	LUMO [eV]	HOMO [eV]	μ_e^{SCLC} [cm^2 V^{-1} s^{-1}]	$L_{c(010)}^{OOP}$ [nm]
PBDB-T	46.0	1.8	621	1.79	−3.52	−5.60	–	–
PYTS-0.0	17.4	2.3	796	1.41	−4.28	−5.88	9.4×10^{-5}	2.09
PYTS-0.1	11.4	2.2	792	1.40	−4.24	−5.89	1.7×10^{-4}	2.34
PYTS-0.3	13.1	2.9	793	1.41	−4.20	−5.89	4.8×10^{-4}	2.53
PYTS-0.5	10.5	2.7	794	1.40	−4.19	−5.88	5.7×10^{-5}	2.45
PYTS-1.0	9.3	3.5	790	1.44	−4.17	−5.87	4.7×10^{-6}	2.18

[a]Obtained from Figure S1c (Supporting Information); [b]calculated as $1240/\lambda_{onset}^{film}$.

which indicates that the FCBS has no significant influence on the conjugation length (Figure S1c, Supporting Information). This is presumably because the effective conjugation length can be reached with very small number of repeating units due to the large and highly fused ladder-type SMA building block (Y5-OD).[46] In addition, the absorption ranges of the P_As were complementary with that of the P_D regardless of the FCBS content, enabling efficient light-harvesting of the all-PSCs (Figure S1c, Supporting Information).

To investigate the P_A aggregation property depending on the FCBS unit content, the temperature-dependent UV–vis absorption spectra in CB solution were measured (Figure S3, Supporting Information).[28,47–50] PYTS-0.0, PYTS-0.1, and PYTS-0.3 exhibited blueshifted absorption maxima and gradually decreased absorption intensity as temperature increased, which indicates that the P_As tend to being aggregated at room temperature, but being disaggregated at high temperatures.[51] However, PYTS-0.0 has the lowest solubility and merely soluble even in hot CB solution (Figure S2 and Table S1, Supporting Information). Thus, PYTS-0.0 polymers quickly form a gel (aggregation even at 80 °C) even before the start of the spin-coating for film preparation, which is attributed to their strong intermolecular π–π interactions.[46,52] The solubilities of P_As were significantly improved with increasing FCBS content. For example, PYTS-1.0 showed increased absorption intensity with large blueshifts of the absorption wavelengths (33 nm) when the temperature increased from 20 to 80 °C (Figure S3e, Supporting Information). The broad absorption spectrum of this polymer at 20 °C indicates that it has multi-molecular conformations and more twisted structures rendered by the flexible spacers, and thus less aggregation in solution. Therefore, we assumed that PYTS-1.0 cannot form aggregated structures during the film forming process, leading to films with less ordered structures and poor electron mobility (will be discussed later). In comparison, the FCBS in PYTS-0.1 and PYTS-0.3 delivered an optimal tradeoff between the solubility and the aggregation in the solution, allowing the formation of well-ordered aggregate structures of the polymers in the films.

To investigate the effects of the FCBS units on the P_A crystallinity and charge-transport properties, grazing-incidence wide-angle X-ray scattering (GIWAXS) and space charge limited current (SCLC) electron mobility (μ_es) measurements were performed (Figure 1e, Figures S4 and S5: Supporting Information). In the GIWAXS profiles, all the polymers showed the face-on preferential packing structures with prominent (100) peaks in the in-plane (IP) direction and (010) peaks in the out-of-plane (OOP) direction, which is beneficial for facilitating vertical charge transport in the thin film (Figures S4 and S5, Supporting Information). Interestingly, the P_As with appropriate FCBS contents show optimal crystallinity and μ_es compared with the P_A without the FCBS unit (Table 1). For details, the coherence lengths (L_cs) of the (010) peaks in the OOP direction estimated from the GIWAXS linecuts increased from 2.09 nm for PYTS-0.0 to 2.53 nm for PYTS-0.3. Accordingly, the SCLC μ_e values increased from 9.4×10^{-5} cm^2 V^{-1} s^{-1} for PYTS-0.0 to 4.8×10^{-4} cm^2 V^{-1} s^{-1} for PYTS-0.3. However, excessive interposition of the FCBS units reduced the crystallinity and μ_es of the P_A. For instance, the $L_{c(010)}^{OOP}$ value decreased to 2.18 nm, and the corresponding μ_e decreased to 4.7×10^{-6} cm^2 V^{-1} s^{-1} for

PYTS-1.0. These results demonstrate that the appropriate incorporation of the FCBS units (0.1 and 0.3 mole fractions) into the P_As can noticeably enhance the crystallinity and charge-transport abilities in thin films, while effectively alleviating their backbone rigidities and aggregation in solutions. However, the introduction of a large amount of FCBS (over 0.5 mole fraction) not only impedes charge transport along polymer backbones but also suppresses the molecular aggregation in the film, thus significantly decreasing the electron mobility of the resulting blends.[53,54]

To characterize the PV properties of the P_As, all-PSCs with a normal type device architecture were fabricated. The detailed device configurations and the fabrication procedures are described in the Supporting Information. **Figure 2**a shows the current density–voltage (J–V) characteristics of the all-PSCs under optimized conditions, and the summarized PV parameters are shown in **Table 2**. The all-PSC device based on the PBDB-T:PYTS-0.0 blend showed a PCE of 13.01% with an open-circuit voltage (V_{oc}) of 0.92 V and a J_{sc} of 22.38 mA cm^{-2}, which is comparable to the reported values.[55] Notably, the all-PSCs with PBDB-T:PYTS-0.3 blend showed a remarkably high PCE of 14.68% with a high J_{sc} of 22.91 mA cm^{-2}, and FF of 0.70. However, the blends with high content of the FCBS units exhibited significantly low performances (with a PCE of 1.71% for the PBDB-T:PYTS-1.0-based device). The origin of the different performances of the blends came from their variations in J_{sc} and FF values. This demonstrates that the FCBS has a strong influence on the PV performance of all-PSCs. The external quantum efficiency (EQE) results are shown in Figure 2b. The calculated J_{sc} values from the EQE spectra are presented in Table 2, which are well-matched with the device J_{sc}s within a deviation of ± 4%. The EQE spectra of the PBDB-T:PYTS-0.1 and PBDB-T:PYTS-0.3 blends showed higher responses in both P_D (550–700 nm) and P_A absorption ranges (750–900 nm) than those of PBDB-T:PYTS-0.0, suggesting that the blend with P_As having proper FCBS units have more efficient charge generations from both P_D and P_A absorption ranges.

To elucidate the origins of different all-PSC performances, their charge-generation, charge-transport, and charge-recombination properties were investigated. First, the photocurrent density (J_{ph}) under effective voltage (V_{eff}) were measured to analyze the charge generation property of the blends. The exciton dissociation probability ($P(E,T)$) values were calculated by the J_{sc} values over the saturation current densities (J_{sat}, at V_{eff} = 3 V).[56] The $P(E,T)$ values increased from 86.8% for the PBDB-T:PYTS-0.0 blend to 91.1% for the PBDB-T:PYTS-0.3 blend, and decreased to 52.8% for the PBDB-T:PYTS-1.0 blend (Figure 2c). This indicates that the interposition of proper mole fraction of the FCBS units in the P_As attained maximum charge generation properties within the PBDB-T:PYTS series. Also, the PBDB-T:PYTS-0.3 blend showed the highest photoluminescence (PL) quenching efficiency (Φ_q) among the blends, supporting the efficient charge separation ability of the PBDB-T:PYTS-0.3 blend (Figure S6, Supporting Information). For example, the Φ_q values of PBDB-T:PYTS-0.0, PBDB-T:PYTS-0.3, and PBDB-T:PYTS-1.0 blends excited at 514 nm were 74.4%, 82.1%, and 41.7%, respectively.

Next, SCLC mobilities for the blend films were measured to investigate charge-transport properties (Table S2, Supporting
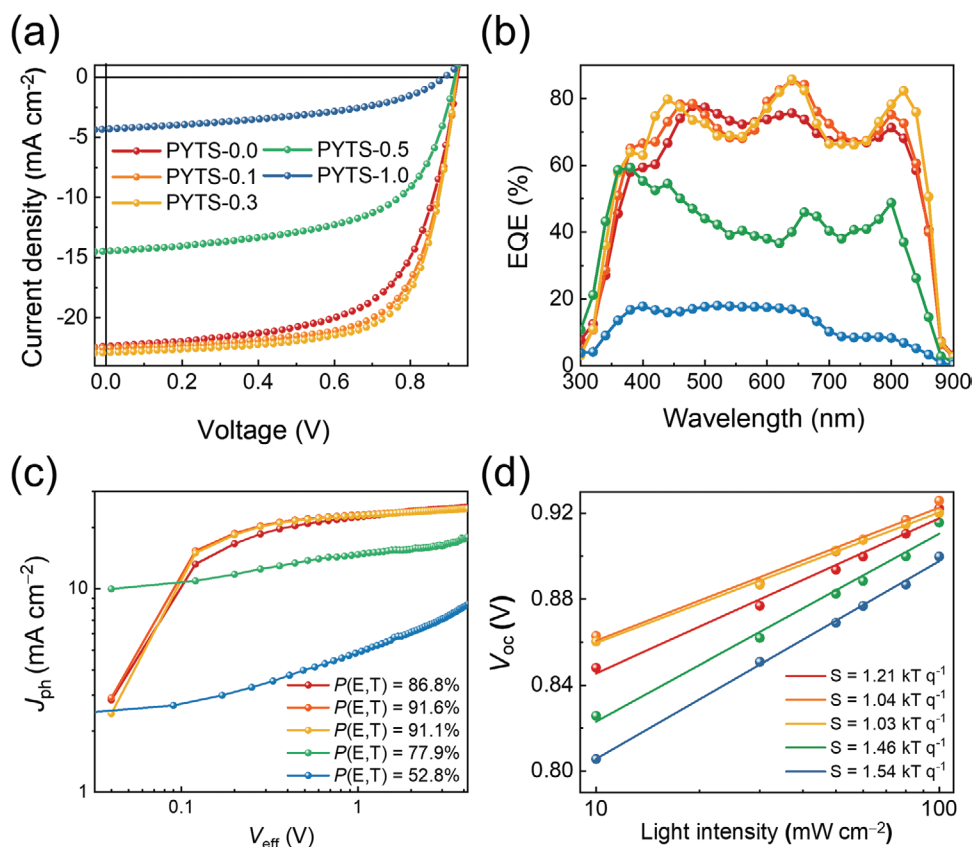
Figure 2. a) J–V curves; b) EQE response spectra; c) J_{ph} versus V_{eff} curves, and d) dependency of V_{oc} on light intensity of the all-PSCs.

Information). The hole mobility (μ_h) values remained almost constant independent on the blends, whereas the μ_e values showed a non-linear trend. For example, μ_e values of the PBDB-T:PYTS-0.0, PBDB-T:PYTS-0.3, and PBDB-T:PYTS-1.0 were 5.8×10^{-5}, 2.3×10^{-4}, and 8.8×10^{-7} cm^2 V^{-1} s^{-1}, respectively. As a result, the PBDB-T:PYTS-0.3 blend showed the most balanced μ_h/μ_e value (1.5) among all the blends including the PBDB-T:PYTS-0.0 blend ($\mu_h/\mu_e = 6.7$), and the PBDB-T:PYTS-1.0 ($\mu_h/\mu_e = 420.5$). Highly unbalanced μ_h/μ_e and very low μ_e of the PBDB-T:PYTS-1.0 blend might be caused by the un-optimized blend morphology and the absence of the electron transport channel. This is also supported by significant difference of μ_e values between the pristine PYTS-1.0 and the PBDB-T:PYTS-1.0 blend. In contrast, the high μ_e value and the balanced μ_h/μ_e of the PBDB-T:PYTS-0.3 blend implies the formation of a well-connected charge-transport pathway in the blend. These high

and balanced charge mobilities result in suppressed charge recombinations, explaining the highest J_{sc} and FF value in the PBDB-T:PYTS-0.3-based all-PSC.

In series, the dependence of J_{sc} and V_{oc} on light intensity (P) was studied to analyze the charge recombination properties of the all-PSCs (Figure S7 (Supporting Information) and Figure 2d). There were no significant differences in the α values (slopes in the J_{sc} vs P plots) across the blends, suggesting that the extent of bimolecular recombination was similar among all the blends (Figure S7, Supporting Information).[57] V_{oc} is proportional to the natural logarithm of P ($V_{oc} = S \times \ln(P)$), and the S value has a unit of kT q^{-1} (where k is the Boltzmann constant, T is temperature, and q refers to elementary charge), being close to the unity when monomolecular/trap-assisted recombinations are not prevalent.[58] The S values exhibited noticeable differences among the blends (Figure 2d).

Table 2. PV performances of the all-PSCs depending on the FCBS compositions in P$_A$s.

P$_A$	V_{oc} [V][a]	J_{sc} [mA cm^{-2}][a]	Calc. J_{sc} [mA cm^{-2}]	FF[a]	PCE$_{max (avg)}$ [%][a]
PYTS-0.0	0.92	22.38	21.51	0.63	13.01 (12.82)
PYTS-0.1	0.92	22.52	22.06	0.68	14.19 (14.04)
PYTS-0.3	0.92	22.91	22.17	0.70	14.68 (14.35)
PYTS-0.5	0.92	14.46	14.09	0.60	7.91 (7.68)
PYTS-1.0	0.89	4.31	4.08	0.44	1.71 (1.64)

[a]All parameters represent average values measured from more than ten all-PSC devices.

**ADVANCED
SCIENCE NEWS**

www.advancedsciencenews.com

**ADVANCED
MATERIALS**

www.advmat.de

For example, the S value decreased from 1.21 kT q^{-1} for PBDB-T:PYTS-0.0 to 1.03 kT q^{-1} for PBDB-T:PYTS-0.3. Then, it significantly increased to 1.54 kT q^{-1} for PBDB-T:PYTS-1.0 blend. This shows that incorporating small amount (less than 0.3 mole fraction) of FCBS units in the P_As suppressed monomolecular or trap-assisted recombination of the all-PSCs, whereas the excessive incorporation (larger than 0.5 mole fraction) rather provoked charge recombination. The combined results from the charge generation and recombination properties support the increased J_{sc} and FF values in the PBDB-T:PYTS-0.1 and PBDB-T:PYTS-0.3 blends compared with those of the PBDB-T:PYTS-0.0 and PBDB-T:PYTS-1.0 blends.

2.2. Thin-Film Mechanical Properties

We analyzed the mechanical properties of the blends using a pseudo free-standing tensile test method. This testing method permits the measurement of the intrinsic tensile property of the thin-film by excluding the influences of the thick substrates.[59] The PBDB-T:P_A blend thin-films were fabricated under the conditions used for the all-PSC fabrication, and the results from the tensile tests are displayed in **Figure 3** and **Table 3**. In overall, as the FCBS content in the P_As increased, the elastic moduli (E) of the resulting blend films increased, suggesting that the FCBS units in the P_As increased the stiffness of the thin-films (Figure 3b). The PBDB-T:PYTS-0.3 blend

showed the highest stretchability with its COS values of 21.64% among the blends, which is superior to that of the blend based on the PYTS-0.0 (COS = 18.84%). In addition, the PBDB-T:PYTS-0.3 blend had a higher toughness value of 3.86 MJ m^{-3} than that of the PBDB-T:PYTS-0.0 blend (2.70 MJ m^{-3}). Further increasing the FCBS content to 0.5 and 1.0 mole fraction in the P_As resulted in increased stress values under the same strains, but they decreased the stretchability of the blend films. It is worthwhile to note that the PYTS-0.3-based all-PSCs attained a high COS value of 21.64% while gaining a high PCE of 14.68% simultaneously. In contrast, most of the PSCs reported so far showed a trade-off between the photovoltaic performance and mechanical ductility (Figure S8 and Table S3, Supporting information).[17,21,24,36,60,61]

In the optical microscopy (OM) images of the tensile bars before testing, the blend films showed different morphologies depending on the P_As (Figure 3c, upper images). The PBDB-T:PYTS-0.0 blend showed the locally formed but large-sized defects in their film (left image), whereas the PBDB-T:PYTS-0.3 blend showed more uniform and smoother surfaces without the defects or agglomerates in the non-strain image (middle image). In comparison, the PBDB-T:PYTS-1.0 blend (right image) showed many aggregates through the film, but their sizes were smaller than those of the PBDB-T:PTYS-0.0 blend. In the films with 12% strain being applied, the three blends also showed very different morphologies (Figure 3c, lower images). The PBDB-T:PTYS-0.0 and PBDB-T:PTYS-1.0 blends
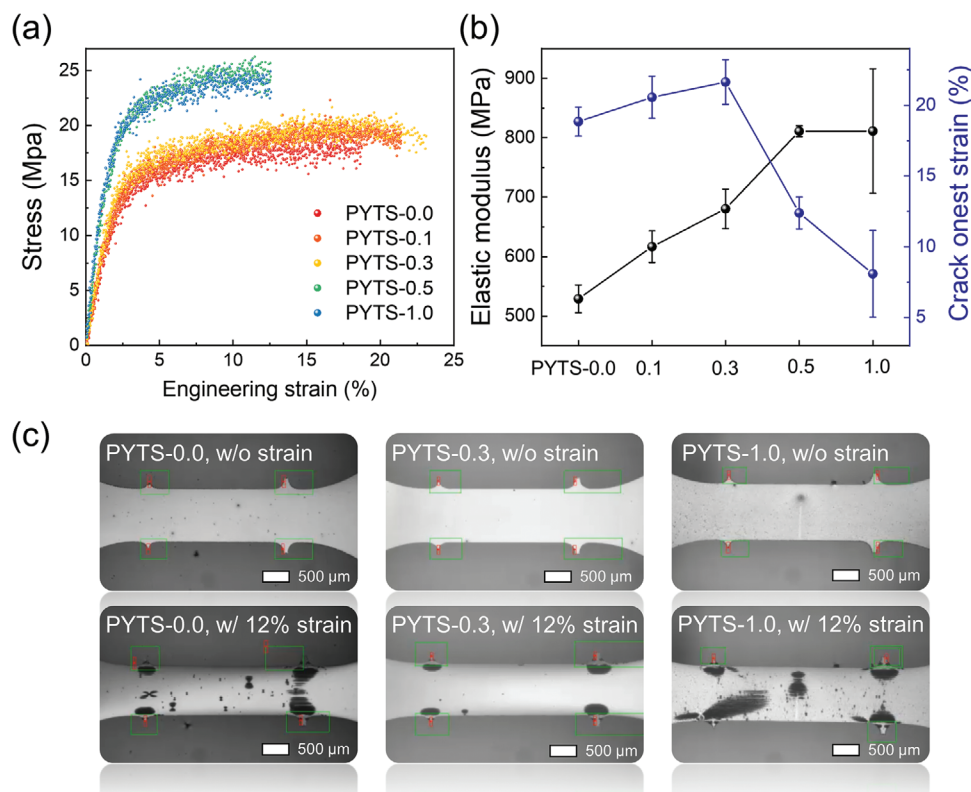
Figure 3. a) Stress–strain curves for the PBDB-T:P_A blends, b) plots of elastic modulus (E) and crack onset strain (COS) values of the blends depending on the PSMAs, and c) tensile-specimen images of the three blends during measurement without strain (upper images) and with 12% engineering strain (lower images); the green and red boxes indicate regimes for displacement tracking by digital image correction (DIC) camera.

Table 3. Mechanical properties of the PBDB-T:P_A blend films measured from the pseudo free-standing tensile test.

P_A	E [MPa][a]	COS [%][a]	Toughness [MJ m^{-3}][a]
PYTS-0.0	529	18.84	2.70
PYTS-0.1	617	20.56	3.28
PYTS-0.3	680	21.64	3.86
PYTS-0.5	811	12.39	2.80
PYTS-1.0	811	8.09	2.64

[a]All parameters represent average values from 3 samples.

showed many cracks being propagated around the defect sites. These cracks and defects accelerated the mechanical failures under further strain due to stress concentrations.[62] In contrast, the PBDB-T:PTYS-0.3 blend showed no such crack propagations, indicating that the film more efficiently dissipated the mechanical stresses under the strains. This result indicates that the FCBS with an optimal amount in the polymer acceptors can provide flexibility to the polymer chains and allow for the formation of the optimal blend morphology without excessive aggregation and phase-separation, leading to the active layers with high mechanical robustness and stretchability.

To further explore the stability of PV properties under cyclic bending, we fabricated flexible all-PSC devices based on PBDB-T:PYTS-0.0 and PBDB-T:PYTS-0.3 blends (Figure S9, Supporting Information). As shown in Figure S9b (Supporting Information), the PBDB-T:PYTS-0.3-based flexible all-PSCs exhibited an initial PCE of 11.04%, which is higher than that of the PBDB-T:PYTS-0.0-based flexible all-PSCs (PCE = 10.12%). In addition, we measured the PCE variations of the flexible devices under continuously bending cycles with a radius of 4 mm. The PBDB-T:PYTS-0.3-based all-PSCs exhibited a higher stability than the PBDB-T:PYTS-0.0-based devices. For example, the PBDB-T:PYTS-0.3-based all-PSCs maintained a 88% of the initial PCE after 350-times bending, while the PCE of the PBDB-T:PYTS-0.0-based devices decreased to the 80% of its initial PCE after the same bending cycles (Figure S9c, Supporting Information).

Moreover, the thermal stabilities of the devices based on the PBDB-T:PYTS-0.0 and PBDB-T:PYTS-0.3 blends at 120°C were compared (Figure S10, Supporting Information). The temperature was selected to accelerate the stability test, referring to the other literatures.[63–66] Both the blends show good morphological stability and retained over 80% of the initial PCEs after 120 h of the thermal testing. This result suggests that all-PCSs based on the PSMAs with and without FCBS units have good morphological stabilities under thermal stresses.
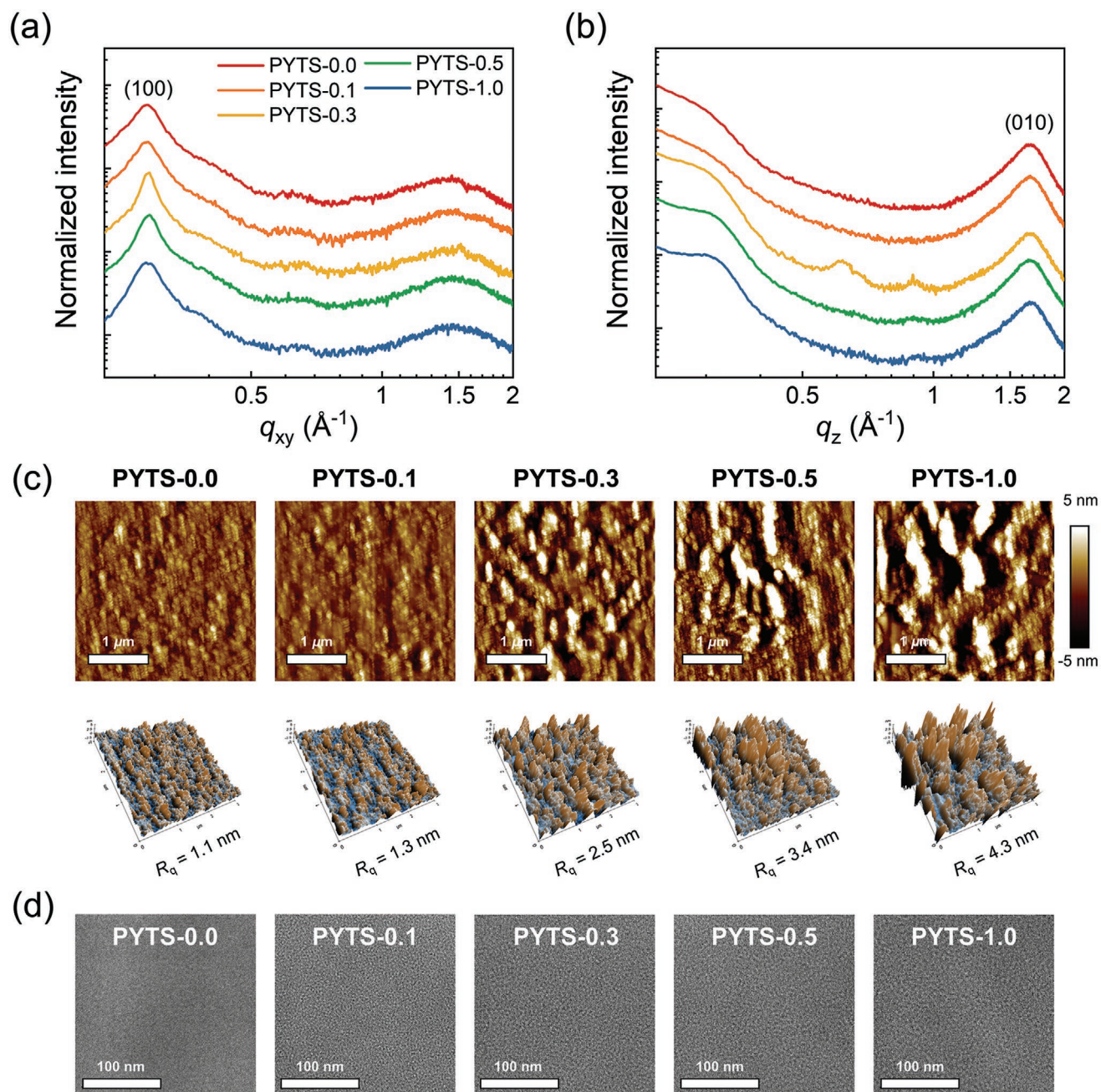
2.3. Morphological Properties

To elucidate the origins of the different photovoltaic and mechanical properties of the PBDB-T:P_A blends, we examined the morphological properties of the blend films using the combined measurements of GIWAXS, atomic force microscopy (AFM), and transmission electron microscopy (TEM) (**Figure 4** and Figures S11–12: Supporting Information). The PBDB-T:P_A

blends showed the non-linear trends of the L_c values from the GIWAXS measurements, being consistent with the crystalline properties of the pristine P_As. As shown in Figure 4a,b and **Table 4**, the L_c values of the (100) peaks in the IP direction increased from 17.1 nm for the PBDB-T:PYTS-0.0 blend to 27.3 nm for the PBDB-T:PYTS-0.3 blend. Then, the L_c value decreased back to 17.6 nm in the PBDB-T:PYTS-1.0 blend. The L_c values of the (010) peaks in the OOP direction showed a similar, non-linear trend with the IP (100) peaks (Table 4). This result indicates that the proper interposition of the FCBS units in the P_A increased the crystallinity of the P_As in the blends, while the excessive incorporation of FCBS decreased the crystallinity.

In the AFM height images, the root-mean-square averaged surface roughness (R_q) of the blends increased with the FCBS content in the P_As (Figure 4c). The R_q of the blend increased from 1.1 nm for the PBDB-T:PYTS-0.0 blend to 2.5 nm for the PBDB-T:PYTS-0.3 blend, and further to 4.3 nm for the PBDB-T:PYTS-1.0 blend. Also, the sizes of the domains in the AFM height and phase images became larger with increasing FCBS content, indicating that the incorporation of FCBS units in the P_As increased the degree of phase segregation between P_D and P_A (Figure 4c and Figure S12: Supporting Information). The TEM images show a similar trend to those from the AFM results, showing larger and more phase-separated domains in the blends with the P_As having higher FCBS content (Figure 4d).

From the combined results of the above morphological analyses, the PBDB-T:PYTS-0.0 blend showed less phase-separated domains compared with those of the PBDB-T:PYTS-0.5 and PBDB-T:PYTS-1.0 blends. However, the PBDB-T:PYTS-0.0 blend contained many defects and large aggregates as observed in the OM images. These were the results of the precipitation of the strongly formed PYTS-0.0 aggregates during the film formation of solution processing due to the highly rigid backbone and low solubility of PYTS-0.0 P_As (left illustration in **Figure 5**). In this case, the largely aggregated P_As in the films deteriorate charge generation and recombination properties of the all-PSCs, and provide crack propagation pathways by acting stress concentration regions when the mechanical stresses are applied. On the other hand, when the excessive amounts of the FCBS units (over 0.5 mole fraction) are incorporated in the P_As, the blend underwent severe phase-separation between P_D and P_A domains, in which much less-ordered P_A structures were formed as indicated by their low crystallinity (right morphology in Figure 5). These disconnected domains with low crystalline structures can limit electron-hopping from domains to other domains, resulting in lower electron mobility and more severe charge recombination and, thus, limiting the J_{sc} and FF of the all-PSCs. Also, the sharp and weak interfaces between the domains can provide crack propagation routes under tensile loadings, resulting in mechanical failures. We speculate that the weak crystalline structures of the PBDB-T:PYTS-0.5 and PBDB-T:PYTS-1.0 were due to the collapsed aggregation of the P_As and their high solubility in the solution. Also, the large phase separation of the blends were formed by liquid–liquid phase separation during the film formation, due to too high solubility of the P_As.[67]

With a proper amount of FCBS units (0.1–0.3 mole fraction) in the P_As, the PBDB-T:PYTS-0.1 and PBDB-T:PYTS-0.3

**ADVANCED
SCIENCE NEWS**

www.advancedsciencenews.com

**ADVANCED
MATERIALS**

www.advmat.de

Figure 4. a,b) GIWAXS linecut profiles in the IP (a) and OOP (b) directions. c) AFM 2D and 3D height images, and d) TEM images of the PBDB-T:P_A blend films.

Table 4. Morphological parameters of the PBDB-T:P_A blends.

P_A	$L_{c(100)}^{IP}$ [nm][a]	$L_{c(010)}^{OOP}$ [nm][a]	R_q^{AFM} [nm][b]
PYTS-0.0	17.1	1.63	1.1
PYTS-0.1	17.7	1.65	1.3
PYTS-0.3	27.3	1.71	2.5
PYTS-0.5	21.9	1.69	3.4
PYTS-1.0	17.6	1.61	4.3

[a]Estimated from the GIWAXS linecut profiles; [b]Obtained from AFM height images.

blends exhibited the optimal extent of phase separation owing to the alleviated P_A backbone rigidities and enhanced solubility compared to PYTS-0.0. More importantly, the highest crystalline properties of P_A are achieved due to their optimal aggregation behaviors in the solution (middle morphology in Figure 5). These morphological features afford the highest electron mobility and the most balanced μ_h/μ_e values in the all-PSCs while the charge recombination is most suppressed. In addition, the smooth film surface of the PBDB-T:PYTS-0.3 blend without defects (precipitated P_A) afforded superior mechanical stretchability and robustness among all the blends. Therefore,
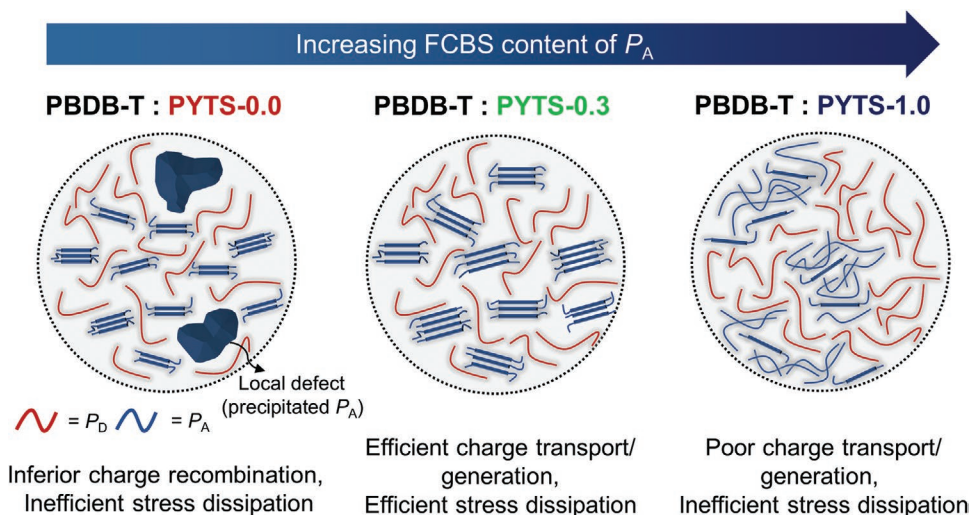
Figure 5. Schematic illustration of the PBDB-T:PYTS-*x* blend morphologies with different PYTS-*x* P$_A$s.

the PBDB-T:PYTS-0.3-based all-PSCs exhibited both a high PCE of 14.68% and excellent mechanical robustness (COS of 21.64%, toughness of 3.86 MJ m^{-3}). Consequently, we note that reducing local defects and preventing excessive phase-separation in the blends are important for achieving high mechanical robustness of thin-films as well as efficient photovoltaic performances in the PSMA-based all-PSCs.

3. Conclusion

We have developed a new series of P$_A$s by embedding FCBS units into the rigid backbones, thereby simultaneously enhancing the PV performance and mechanical resilience of all-PSCs. Incorporation of a proper content (0.1–0.3 mol fraction) of the FCBS segment into the P$_A$ backbone endowed increased backbone flexibility and solubility to the resulting P$_A$s, thereby alleviating chain rigidity and preventing excessive aggregation in the solution. As a result, the all-PSC based on PBDB-T:PYTS-0.3 exhibited a PCE of 14.68% with significantly enhanced J_{sc} and FF, which is superior to that of the devices based on the P$_A$s without FCBS as the results of optimal morphology, enhanced exciton dissociation, and suppressed monomolecular recombination. Moreover, the improved morphological features of the PBDB-T:PYTS-0.3 blend enabled higher mechanical stretchability and robustness with a COS of 21.64% and toughness of 3.86 MJ m^{-3}. Our results demonstrate that FCBS can enhance the PV performance and mechanical robustness of the devices concurrently. This strategy provides a new and simple way to develop highly efficient and mechanically robust all-PSCs appropriate for stretchable and flexible electronics.

Supporting Information

Supporting Information is available from the Wiley Online Library or from the author.

Conflict of Interest

The authors declare no conflict of interest.

Data Availability Statement

The data that support the findings of this study are available from the corresponding author upon reasonable request.

[1] A. Facchetti, *Mater. Today* **2013**, *16*, 123.
[2] J. Choi, W. Kim, S. Kim, T.-S. Kim, B. J. Kim, *Chem. Mater.* **2019**, *31*, 9057.
[3] G. Wang, F. S. Melkonyan, A. Facchetti, T. J. Marks, *Angew. Chem., Int. Ed.* **2019**, *58*, 4129.

ADVANCED
SCIENCE NEWS
www.advancedsciencenews.com

ADVANCED
MATERIALS
www.advmat.de

[4] F. Peng, K. An, W. Zhong, Z. Li, L. Ying, N. Li, Z. Huang, C. Zhu, B. Fan, F. Huang, Y. Cao, *ACS Energy Lett.* **2020**, *5*, 3702.

[5] Z. Luo, T. Liu, R. Ma, Y. Xiao, L. Zhan, G. Zhang, H. Sun, F. Ni, G. Chai, J. Wang, C. Zhong, Y. Zou, X. Guo, X. Lu, H. Chen, H. Yan, C. Yang, *Adv. Mater.* **2020**, *32*, 2005942.

[6] Q. Fan, H. Fu, Q. Wu, Z. Wu, F. Lin, Z. Zhu, J. Min, H. Y. Woo, A. K.-Y. Jen, *Angew. Chem., Int. Ed.* **2021**, *60*, 15935.

[7] T. Liu, T. Yang, R. Ma, L. Zhan, Z. Luo, G. Zhang, Y. Li, K. Gao, Y. Xiao, J. Yu, X. Zou, H. Sun, M. Zhang, T. A. Dela Peña, Z. Xing, H. Liu, X. Li, G. Li, J. Huang, C. Duan, K. S. Wong, X. Lu, X. Guo, F. Gao, H. Chen, F. Huang, Y. Li, Y. Li, Y. Cao, B. Tang, H. Yan, *Joule* **2021**, *5*, 914.

[8] T. Jia, J. Zhang, W. Zhong, Y. Liang, K. Zhang, S. Dong, L. Ying, F. Liu, X. Wang, F. Huang, Y. Cao, *Nano Energy* **2020**, *72*, 104718.

[9] H. Fu, Y. Li, J. Yu, Z. Wu, Q. Fan, F. Lin, H. Y. Woo, F. Gao, Z. Zhu, A. K. Jen, *J. Am. Chem. Soc.* **2021**, *143*, 2665.

[10] B. Liu, H. Sun, J.-W. Lee, J. Yang, J. Wang, Y. Li, B. Li, M. Xu, Q. Liao, W. Zhang, D. Han, L. Niu, H. Meng, B. J. Kim, X. Guo, *Energy Environ. Sci.* **2021**, *14*, 4499.

[11] H. Sun, B. Liu, Y. Ma, J.-W. Lee, J. Yang, J. Wang, Y. Li, B. Li, K. Feng, Y. Shi, B. Zhang, D. Han, H. Meng, L. Niu, B. J. Kim, Q. Zheng, X. Guo, *Adv. Mater.* **2021**, *33*, 2102635.

[12] Z. G. Zhang, Y. Yang, J. Yao, L. Xue, S. Chen, X. Li, W. Morrison, C. Yang, Y. Li, *Angew. Chem., Int. Ed.* **2017**, *56*, 13503.

[13] H. Yao, F. Bai, H. Hu, L. Arunagiri, J. Zhang, Y. Chen, H. Yu, S. Chen, T. Liu, J. Y. L. Lai, Y. Zou, H. Ade, H. Yan, *ACS Energy Lett.* **2019**, *4*, 417.

[14] J. Wu, Y. Meng, X. Guo, L. Zhu, F. Liu, M. Zhang, *J. Mater. Chem. A* **2019**, *7*, 16190.

[15] R. Sun, W. Wang, H. Yu, Z. Chen, X. Xia, H. Shen, J. Guo, M. Shi, Y. Zheng, Y. Wu, W. Yang, T. Wang, Q. Wu, Y. Yang, X. Lu, J. Xia, C. J. Brabec, H. Yan, Y. Li, J. Min, *Joule* **2021**, *5*, 1548.

[16] D. K. Tran, A. Robitaille, I. J. Hai, X. Ding, D. Kuzuhara, T. Koganezawa, Y.-C. Chiu, M. Leclerc, S. A. Jenekhe, *J. Mater. Chem. A* **2020**, *8*, 21070.

[17] J.-W. Lee, C. Sun, B. S. Ma, H. J. Kim, C. Wang, J. M. Ryu, C. Lim, T.-S. Kim, Y.-H. Kim, S.-K. Kwon, B. J. Kim, *Adv. Energy Mater.* **2021**, *11*, 2003367.

[18] W. Lee, J.-H. Kim, T. Kim, S. Kim, C. Lee, J.-S. Kim, H. Ahn, T.-S. Kim, B. J. Kim, *J. Mater. Chem. A* **2018**, *6*, 4494.

[19] Y. U. Kim, B. S. Ma, Y. Kim, S. H. Park, H. Kang, H. J. Yoon, M. J. Cho, T.-S. Kim, J. H. Kim, D. H. Choi, *Chem. Eng. J.* **2021**, *415*, 128952.

[20] Z. G. Zhang, Y. Li, *Angew. Chem., Int. Ed.* **2021**, *60*, 4422.

[21] Q. Fan, W. Su, S. Chen, W. Kim, X. Chen, B. Lee, T. Liu, U. A. Méndez-Romero, R. Ma, T. Yang, W. Zhuang, Y. Li, Y. Li, T.-S. Kim, L. Hou, C. Yang, H. Yan, D. Yu, E. Wang, *Joule* **2020**, *4*, 658.

[22] H. Sun, H. Yu, Y. Shi, J. Yu, Z. Peng, X. Zhang, B. Liu, J. Wang, R. Singh, J. Lee, Y. Li, Z. Wei, Q. Liao, Z. Kan, L. Ye, H. Yan, F. Gao, X. Guo, *Adv. Mater.* **2020**, *32*, 2004183.

[23] C. R. McNeill, *Energy Environ. Sci.* **2012**, *5*, 5653.

[24] Q. Wu, W. Wang, Y. Wu, Z. Chen, J. Guo, R. Sun, J. Guo, Y. Yang, J. Min, *Adv. Funct. Mater.* **2021**, *31*, 2010411.

[25] R. Sun, J. Guo, Q. Wu, Z. Zhang, W. Yang, J. Guo, M. Shi, Y. Zhang, S. Kahmann, L. Ye, X. Jiao, M. A. Loi, Q. Shen, H. Ade, W. Tang, C. J. Brabec, J. Min, *Energy Environ. Sci.* **2019**, *12*, 3118.

[26] J. Du, K. Hu, J. Zhang, L. Meng, J. Yue, I. Angunawela, H. Yan, S. Qin, X. Kong, Z. Zhang, B. Guan, H. Ade, Y. Li, *Nat. Commun.* **2021**, *12*, 5264.

[27] Z. Li, X. Xu, W. Zhang, X. Meng, W. Ma, A. Yartsev, O. Inganäs, M. R. Andersson, R. A. J. Janssen, E. Wang, *J. Am. Chem. Soc.* **2016**, *138*, 10935.

[28] Y. Wu, S. Schneider, C. Walter, A. H. Chowdhury, B. Bahrami, H.-C. Wu, Q. Qiao, M. F. Toney, Z. Bao, *J. Am. Chem. Soc.* **2020**, *142*, 392.

[29] Z. Genene, W. Mammo, E. Wang, M. R. Andersson, *Adv. Mater.* **2019**, *31*, 1807275.

[30] D. Chen, S. Liu, J. Liu, J. Han, L. Chen, Y. Chen, *ACS Appl. Polym. Mater.* **2021**, *3*, 1923.

[31] J.-W. Lee, M. J. Sung, D. Kim, S. Lee, H. You, F. S. Kim, Y.-H. Kim, B. J. Kim, S.-K. Kwon, *Chem. Mater.* **2020**, *32*, 2572.

[32] J. Du, K. Hu, L. Meng, I. Angunawela, J. Zhang, S. Qin, A. Liebman-Pelaez, C. Zhu, Z. Zhang, H. Ade, Y. Li, *Angew. Chem., Int. Ed.* **2020**, *132*, 15293.

[33] J. Du, K. Hu, L. Meng, I. Angunawela, J. Zhang, S. Qin, A. Liebman-Pelaez, C. Zhu, Z. Zhang, H. Ade, Y. Li, *Angew. Chem., Int. Ed.* **2020**, *59*, 15181.

[34] J. Mun, G.-J. N. Wang, J. Y. Oh, T. Katsumata, F. L. Lee, J. Kang, H.-C. Wu, F. Lissel, S. Rondeau-Gagné, J. B.-H. Tok, Z. Bao, *Adv. Funct. Mater.* **2018**, *28*, 1804222.

[35] A. Chortos, Z. Bao, *Mater. Today* **2014**, *17*, 321.

[36] Y. Wang, Q. Zhu, H. B. Naveed, H. Zhao, K. Zhou, W. Ma, *Adv. Energy Mater.* **2020**, *10*, 1903609.

[37] Q. Fan, W. Su, S. Chen, T. Liu, W. Zhuang, R. Ma, X. Wen, Z. Yin, Z. Luo, X. Guo, L. Hou, K. Moth-Poulsen, Y. Li, Z. Zhang, C. Yang, D. Yu, H. Yan, M. Zhang, E. Wang, *Angew. Chem., Int. Ed.* **2020**, *59*, 19835.

[38] Q. Fan, R. Ma, T. Liu, J. Yu, Y. Xiao, W. Su, G. Cai, Y. Li, W. Peng, T. Guo, Z. Luo, H. Sun, L. Hou, W. Zhu, X. Lu, F. Gao, E. Moons, D. Yu, H. Yan, E. Wang, *Sci. China: Chem.* **2021**, *64*, 1380.

[39] N. Kazerouni, E. L. Melenbrink, P. Das, B. C. Thompson, *ACS Appl. Polym. Mater.* **2021**, *3*, 3028.

[40] J.-W. Lee, D. Jeong, D. J. Kim, T. N.-L. Phan, J. S. Park, T.-S. Kim, B. J. Kim, *Energy Environ. Sci.* **2021**, *14*, 4067.

[41] W. Wang, Q. Wu, R. Sun, J. Guo, Y. Wu, M. Shi, W. Yang, H. Li, J. Min, *Joule* **2020**, *4*, 1070.

[42] Z. Zheng, H. Yao, L. Ye, Y. Xu, S. Zhang, J. Hou, *Mater. Today* **2020**, *35*, 115.

[43] J.-W. Lee, B. S. Ma, J. Choi, J. Lee, S. Lee, K. Liao, W. Lee, T.-S. Kim, B. J. Kim, *Chem. Mater.* **2020**, *32*, 582.

[44] F. Panzer, H. Bässler, A. Köhler, *J. Phys. Chem. Lett.* **2017**, *8*, 114.

[45] Z. Hu, R. T. Haws, Z. Fei, P. Boufflet, M. Heeney, P. J. Rossky, D. A. Vanden, Bout, *Proc. Natl. Acad. Sci. USA* **2017**, *114*, 5113.

[46] B. C. Schroeder, Y. C. Chiu, X. Gu, Y. Zhou, J. Xu, J. Lopez, C. Lu, M. F. Toney, Z. Bao, *Adv. Electron. Mater.* **2016**, *2*, 1600104.

[47] N. Wang, Y. Yu, R. Zhao, Z. Ding, J. Liu, L. Wang, *Macromolecules* **2020**, *53*, 3325.

[48] S. Seo, J. Kim, H. Kang, J.-W. Lee, S. Lee, G.-U. Kim, B. J. Kim, *Macromolecules* **2021**, *54*, 53.

[49] Q.-Y. Li, Z.-F. Yao, J.-Y. Wang, J. Pei, *Rep. Prog. Phys.* **2021**, *84*, 076601.

[50] J.-W. Lee, N. Choi, D. Kim, T. N.-L. Phan, H. Kang, T.-S. Kim, B. J. Kim, *Chem. Mater.* **2021**, *33*, 1070.

[51] N. Wang, X. Long, Z. Ding, J. Feng, B. Lin, W. Ma, C. Dou, J. Liu, L. Wang, *Macromolecules* **2019**, *52*, 2402.

[52] H. Hu, P. C. Y. Chow, G. Zhang, T. Ma, J. Liu, G. Yang, H. Yan, *Acc. Chem. Res.* **2017**, *50*, 2519.

[53] Y. Liu, X.-Y. Wang, Z.-Y. Wang, Y. Lu, X.-F. Cheng, B. Tang, J.-Y. Wang, J. Pei, *Polym. Chem.* **2021**, *12*, 370.

[54] T. Erdmann, S. Fabiano, B. Milián-Medina, D. Hanifi, Z. Chen, M. Berggren, J. Gierschner, A. Salleo, A. Kiriy, B. Voit, A. Facchetti, *Adv. Mater.* **2016**, *28*, 9169.

[55] Y. Wu, Q. Wu, W. Wang, R. Sun, J. Min, *Sol. RRL* **2020**, *4*, 2000409.

[56] P. W. M. Blom, V. D. Mihailetchi, L. J. A. Koster, D. E. Markov, *Adv. Mater.* **2007**, *19*, 1551.

[57] L. J. A. Koster, M. Kemerink, M. M. Wienk, K. Maturová, R. A. J. Janssen, *Adv. Mater.* **2011**, *23*, 1670.

[58] S. R. Cowan, A. Roy, A. J. Heeger, *Phys. Rev. B* **2010**, *82*, 245207.

[59] J.-H. Kim, A. Nizami, Y. Hwangbo, B. Jang, H.-J. Lee, C.-S. Woo, S. Hyun, T.-S. Kim, *Nat. Commun.* **2013**, *4*, 2520.

[60] A. D. Printz, D. J. Lipomi, *Appl. Phys. Rev.* **2016**, *3*, 021302.

[61] B. Lin, L. Zhang, H. Zhao, X. Xu, K. Zhou, S. Zhang, L. Gou, B. Fan, L. Zhang, H. Yan, X. Gu, L. Ying, F. Huang, Y. Cao, W. Ma, *Nano Energy* **2019**, *59*, 277.

[62] J.-W. Lee, B. S. Ma, H. J. Kim, T.-S. Kim, B. J. Kim, *JACS Au* **2021**, *1*, 612.

[63] Y. Xu, J. Yuan, S. Liang, J.-D. Chen, Y. Xia, B. W. Larson, Y. Wang, G. M. Su, Y. Zhang, C. Cui, M. Wang, H. Zhao, W. Ma, *ACS Energy Lett.* **2019**, *4*, 2277.

[64] W. Yang, Z. Luo, R. Sun, J. Guo, T. Wang, Y. Wu, W. Wang, J. Guo, Q. Wu, M. Shi, H. Li, C. Yang, J. Min, *Nat. Commun.* **2020**, *11*, 1218.

[65] H. J. Kim, J.-H. Kim, J.-H. Ryu, Y. Kim, H. Kang, W. B. Lee, T.-S. Kim, B. J. Kim, *ACS Nano* **2014**, *8*, 10461.

[66] T. Kim, J. Choi, H. J. Kim, W. Lee, B. J. Kim, *Macromolecules* **2017**, *50*, 6861.

[67] S. Pang, R. Zhang, C. Duan, S. Zhang, X. Gu, X. Liu, F. Huang, Y. Cao, *Adv. Energy Mater.* **2019**, *9*, 1901740.